Journal of Power Sources 194 (2009) 880–885

Contents lists available at ScienceDirect

Journal of Power Sources

journal homepage: www.elsevier.com/locate/jpowsour

Thermal cycle stability of $BaO–B_2O_3–SiO_2$ sealing glass

Lian Peng, QingShan Zhu*

State Key Laboratory of Multi-Phase Complex Systems, Institute of Process Engineering, Chinese Academy of Sciences, Beijing 100190, People's Republic of China

ARTICLE INFO

Article history:
Received 30 April 2009
Accepted 5 June 2009
Available online 16 June 2009

Keywords:
Sealing glass
Leak rates
Thermal cycle stability
Solid oxide fuel cells

ABSTRACT

Thermal cycle stability is very important for glass seals in planar solid oxide fuel cell (pSOFC) applications. In the present study, thermal cycle stability of a thermally stable sealing glass is investigated using a sealing fixture from 150 °C to 700 °C. SS410 alloy with the TEC (thermal expansion coefficient) of $12.2 \times 10^{-6}\,K^{-1}$ (room temperature to 700 °C) is used to evaluate the effect of TEC mismatch on the thermal cycle stability. The leak rates increase with thermal cycles and appear to be two different stages. Microstructure examinations are performed to investigate the degradation mechanism of the thermal cycle stability. It is found that the sealing glass interacts chemically with the SS410 alloy and the formation of $BaCrO_4$ new phase results in the rapid increase of the leak rates.

1. Introduction

Sealing has been identified as one of the most difficult issues for the development of planar solid oxide fuel cells (pSOFCs). The requirements for the sealant are stringent due to the high operating temperature (approximately 700–1000 °C) and the very harsh environments (oxidizing, reducing and humid). The sealant needs to have long-term thermal stability (>40,000 h) at operating temperature and long-term thermal cycle stability (>1000 cycles) during routine operation [1–3]. As a result, much attention has been focused on sealing materials.

Up to the present, three main types of sealing materials, i.e. braze, mica and glass (or glass-ceramic), have been investigated in literatures [4–10]. Among the three materials, glass is the mainly sealant which is extensively investigated. Some important issues, e.g. thermal stability, chemical compatibility and chemical stability, have been investigated for glass seals in detail [11–20]. Sohn et al. [13] investigated the thermal stability of $SiO_2–B_2O_3–BaO–Al_2O_3$ glass and chemical compatibility with electrolyte (8YSZ). They found that the TEC (thermal expansion coefficient) values of their glasses decreased with the formation of celsian. Yang et al. [15] investigated the chemical interactions of $SiO_2–CaO–BaO–B_2O_3–Al_2O_3$ based sealing glasses with oxidation resistant alloys. They found that the formation of $BaCrO_4$ led to the physical separation of the sealing glass from the interconnect alloys due to high thermal expansion mismatch. Larsen et al. [18,19] investigated the chemical stability of phosphate glasses in wet fuel gas and air. They found that the volatility of P_2O_5 resulted in the poor chemical stability of phosphate glasses. Reis and Brow [20] investigated the influence of B_2O_3 content on the chemical stability of borosilicate glasses in wet forming gas. They concluded that the most promising sealing glasses have low B_2O_3 contents. However, thermal cycle stability, which is also very important for SOFC applications, has rarely been investigated for glass seals. Singh [21] developed a long-term thermal cycle stable glass which could endure more than 300 thermal cycles between room temperature (RT) and 800 °C, but the detailed information about the glass composition and interface microstructure analyses was not revealed.

A thermally stable sealing glass in $BaO–B_2O_3–SiO_2$ system has been developed in our earlier papers and the glass was investigated in detail [22,23]. The sealing temperature of the glass was determined to be about 810 °C. The glass has a TEC of $9.9 \times 10^{-6}\,K^{-1}$ between room temperature and 631 °C (dilatometer determined transition temperature). It exhibits long-term thermal stability at 700 °C (500 h) and 800 °C (300 h). It also shows good chemical compatibility with 8YSZ at 700 °C for 500 h. In this paper, the thermal cycle stability of the thermally stable sealing glass was investigated. SS410 alloy was used to evaluate the effect of TEC mismatch on the thermal cycle stability. Effect of thermal cycling on the leak rates of the glass was analyzed in detail. The SS410/glass interface was investigated after thermal cycling and the degradation mechanism of the thermal cycle stability was discussed.

2. Experimental

The glass used in the present work was developed in our earlier papers and has the following composition (mol%): 38.3%SiO_2, 27.4%B_2O_3, 31.3%BaO, 0.6%La_2O_3, 1.6%ZrO_2, 0.8%Y_2O_3 [22,23]. As

* Corresponding author at: State Key Laboratory of Multi-Phase Complex Systems, Institute of Process Engineering, Chinese Academy of Sciences, Zhong Guan Cun, Haidian District, P.O. Box 353, Beijing 100190, People's Republic of China.
Tel.: +86 10 62536108; fax: +86 10 62536108.
E-mail address: qszhu@home.ipe.ac.cn (Q. Zhu).

0378-7753/$ – see front matter © 2009 Elsevier B.V. All rights reserved.
doi:10.1016/j.jpowsour.2009.06.018

the primary constituents, SiO_2 and B_2O_3 can form a special network which exhibits both good thermal stability and a suitable glass transition temperature (T_g). Various oxides were added to tailor different properties of the glass, e.g., BaO to increase TEC, and La_2O_3, ZrO_2 and Y_2O_3 were selectively added to promote chemical compatibility [19]. Our glass has no alkali oxide as a flux because alkali metal ions can easily diffuse into the fuel cell components, leading to interface reaction or to increase electrical conductance [24].

2.1. Raw materials

Reagent grade oxides and carbonates in right proportions were melted on a 10–20 g scale in a Pt crucible at 1250–1400 °C in air for 2–4 h and then naturally cooled to room temperature to obtain glass blocks. The glass block was then cut into pieces and ground into bars with nominal dimensions of 15 mm × 4 mm × 2 mm for TEC characterizations or 25 mm × 2 mm × 2 mm for the thermal cycle test. SS410 alloy, which is a common chromia-forming alloy, was used to evaluate the effect of TEC mismatch on the thermal cycle stability.

2.2. Glass characterization

The as-prepared glass was tested using an X-ray diffractometer (XRD, X'Pert MPD Pro, PANalytical, the Netherlands) with CuK_α radiation to confirm the amorphous nature of the glass, exhibiting two broad haloes in the XRD pattern. The glass after thermal cycling was also tested using the X-ray diffractometer to identify new phase formed.

The TEC of the glass was measured in stagnant air from room temperature up to the glass softening temperature (T_s), via a dilatometer (L75.1550, LINSEIS, Germany) with a heating rate of 10 °C min^{-1}. A total of six specimens were measured for the TEC and the average value was used as the TEC value for the glass. The TEC of the SS410 was also characterized for the purpose of comparison. Thermal properties like the glass transition temperature (T_g) and softening temperature (T_s) were also measured by the dilatometer.

2.3. Chemical reactivity

The glass/SS410 interface was checked using a Field-Emission Scanning Electron Microscopy (SEM, Quanta 200F, the Netherlands) and an associated energy dispersive X-ray spectroscopy (EDX) at an operation voltage of 15 kV to reveal any chemical reactivity and microstructure changes. All of the microscopic images were obtained as back-scattering images. No boron could be detected with the available EDX system, consequently, boron was not considered in detail in the EDX investigations.

2.4. Thermal cycle stability

Thermal cycle stability of the sealing glass was investigated through a leak rate test. The test fixture is illustrated in Fig. 1. Eight glass bars (25 mm × 2 mm × 2 mm) were placed on a SS410 bottom cap (50 mm × 50 mm × 50 mm with a wall thickness of 5 mm) end to end. Two SS304 tubes (ϕ3 mm) were welded into one side of the bottom cap for gas in and out. In order to maintain the height of the sealing glass, a SS410 frame (66 mm × 66 mm × 51 mm) was used. The bottom cap was then embedded in the frame. It is noticed that the height of the frame is 1 mm higher than that of the SS410 bottom cap. A SS410 plate was machined to the desired size (66 mm × 66 mm × 5 mm) and then put on the glass bars. The surfaces of the SS410 bottom cap and SS410 plate were both ground by a 400 grit SiC wheel and rinsed with acetone. The SS410 plate weighs 193 g, so the contact stress for sealing is about 4.93 kPa. When the fixture was heated to 810 °C, the glass began to wet the SS410 plate and bottom cap. Simultaneously, the height of the glass began to decrease due to the weight of the SS410 plate. When the height of the glass decreased to 1 mm, the SS410 plate contacted the frame. Therefore, the height of the glass remained 1 mm.

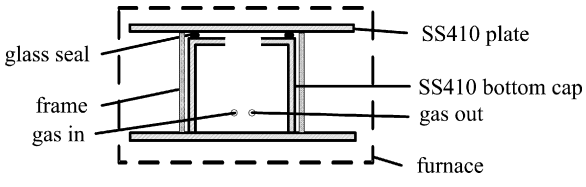

Fig. 1. A schematic diagram of the thermal cycle test fixture.

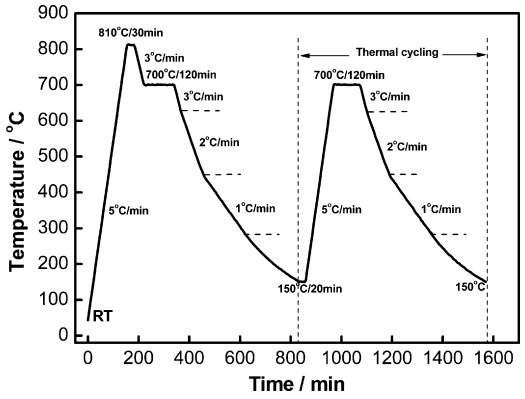

Fig. 2. A temperature profile for thermal cycling.

The fixture was first heated at a heating rate of 5 °C min^{-1} to 810 °C for 0.5 h in order to make the glass wet the SS410 metals and then cooled at a cooling rate of 3 °C min^{-1} to 700 °C for 2 h. At 700 °C, the decay in pressure was measured and the leak rate was calculated for the 0th thermal cycle. After the first dwell at 700 °C for 2 h, the sample was cooled to 630 °C at a cooling rate of 3 °C min^{-1}, to 450 °C at a cooling rate of 2 °C min^{-1}, to 280 °C at a cooling rate of 1 °C min^{-1} and furnace cooled to 150 °C for 20 min to initiate thermal cycling. The temperature profile for the thermal cycling is shown in Fig. 2. Each thermal cycle took about 12 h, allowing two cycles to be conducted each day. The gas used in this study was ambient air (relative humidity of 30% at 25 °C, corresponding to H_2O partial pressure of 9.45×10^2 Pa).

The known-volume (75 cm^3) bottom cap was kept in a furnace and connected to a pressure sensor via a ϕ3 mm SS304 tube and a silicone rubber tube. The volume of the SS304 tubes and silicone rubber tubes is around 8% of the volume of the bottom cap, so the volume of the SS304 tubes and silicone rubber tubes is small enough to be omitted. By setting up a differential pressure (initially ~8 kPa) in the system after dwelling at 700 °C for 1 h in each thermal cycle, the leak rate was measured by monitoring the pressure change with time. According to the Fick's law of diffusion, the leak rate L (kPa min^{-1}) changes with pressure P (kPa) according to the equation (1):

$$L = -\frac{dP}{dt} = kP \quad (1)$$

where t is time (min), k is a constant for a specific thermal cycle. If Eq. (1) is integrated, Eq. (2) can be achieved:

$$\ln P = -k \cdot t + c \quad (2)$$

where c is also a constant. According to Eq. (2), the parameters k and c can be achieved by the plot of $\ln P$ versus t. After k has been determined, the leak rate L (i.e. $-dP/dt$, kPa min^{-1}) under a definite differential pressure can be calculated according to Eq. (1). In our

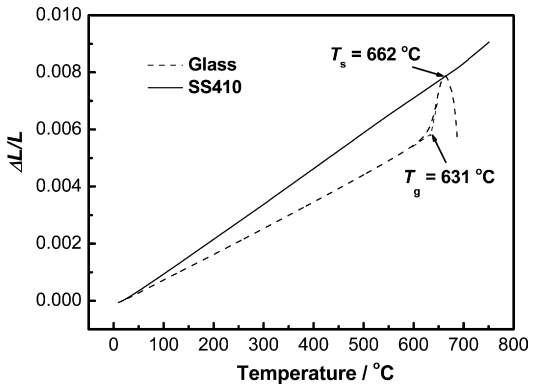

Fig. 3. Thermal expansion behaviors of the newly developed sealing glass and SS410 (heating rate of 10 °C min^{-1}, in air).

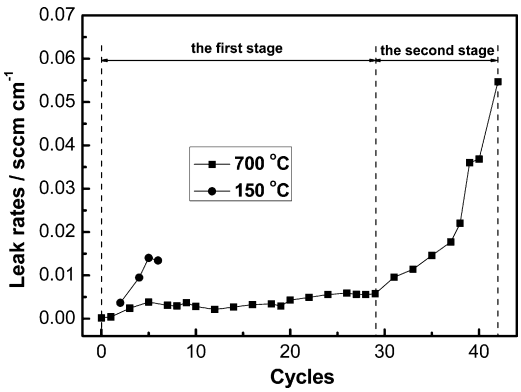

Fig. 4. Dependence of the leak rates (at a differential of 1.379 kPa) on thermal cycles.

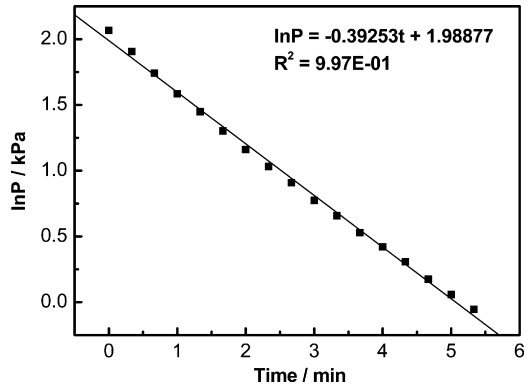

Fig. 5. Actual ln P versus t data at 700 °C and a corresponding linear fitting result for the 27th thermal cycle.

experiments, the leak rate under a differential pressure of 1.379 kPa was calculated for each thermal cycle because this low differential pressure may be appropriate for the planar SOFC stacks with Ni/YSZ anode-supported thin electrolyte cells [25]. The leak rate L is further normalized with respect to the outer leak length (20 cm) of the glass seal and converted into L' (leak rate in standard cubic centimeters per minute per leak length at STP, sccm cm^{-1}) by Eq. (3):

$$L' = \frac{L \times 1000 \times V \times 22.4 \times 1000}{20 \times R \times T} \quad (3)$$

where V (m^3) is the volume of the bottom cap, R (J mol^{-1} K^{-1}) the gas constant, T (K) is the operating temperature.

3. Results and discussion

3.1. Thermal properties

Fig. 3 shows a typical thermal expansion curve of the newly developed glass together with that of the SS410, where the TEC value of the glass was calculated to be 9.9×10^{-6} K^{-1} between room temperature and 631 °C (dilatometer determined T_g). The TEC value of the SS410 was calculated to be 12.2×10^{-6} K^{-1} in the same temperature range. The glass transition temperature (631 °C) is lower than the operation temperature (i.e. 700 °C), which would be beneficial to thermal stress release at operating temperature since significant stress begins to develop only as temperature drops below T_g [3]. It is noticed that the glass soften temperature (T_s, 662 °C) is also lower than 700 °C, which is beneficial to crack heal at operating temperature [21].

3.2. Thermal cycle stability

The dependence of the leak rates at 700 °C on thermal cycles is shown in Fig. 4. Fig. 5 shows the actual ln P versus t data at 700 °C and the corresponding linear fitting result for the 27th thermal cycle. It is interesting to note from Fig. 4 that before thermal cycling, the 700 °C leak rate of the glass seal was 1.8×10^{-4} sccm cm^{-1} (the 0th thermal cycle). This value is very low and demonstrates that the sealing is successful. Therefore, the leak rate of the 0th thermal cycle can be determined to be the background leak rate. Ideally, the leak rate of the background should be zero. In reality, the actual low leak rate was limited by the system's background since there were tube connectors in the setup.

The dependence of the leak rates at 150 °C on thermal cycles is also shown in Fig. 4. It is noticed from Fig. 4 that the 150 °C leak rate of the glass seal is higher than the 700 °C leak rate for the same thermal cycle. This phenomenon can be explained by the "self-healing" behavior of the glass [21]. Cracks occurred in the bulk of the glass and at the glass/SS410 interface upon heating and cooling because of the large TEC mismatch between the glass and SS410. At 150 °C, the cracks could not "heal" due to the high viscosity of the glass. When the glass was heated to 700 °C (above T_s), the cracks could "heal", which resulted in the lower leak rates. The 150 °C leak rate was so high that the pressure data could not be achieved after six thermal cycles, so the 150 °C leak rate was not calculated after six thermal cycles.

It is noticed from Fig. 4 that the 700 °C leak rates increased with thermal cycles. After 42 thermal cycles, the leak rate of the glass reached to be 5.5×10^{-2} sccm cm^{-1}, which is far higher than the initial leak rate (1.8×10^{-4} sccm cm^{-1}). In order to investigate the degradation mechanism of the leak rates, the microstructure of the glass/SS410 interface after 42 thermal cycles was examined.

The photo of the fixture after 42 thermal cycles is shown in Fig. 6. It is noticed that some new phase was formed between the glass and SS410 and certain part of glass had peeled from the SS410. The XRD pattern of the peeling glass was shown in Fig. 7, which shows the presence of $BaCrO_4$.

The SS410/glass interface after 42 thermal cycles was cut and polished to investigate interface reaction. The microstructure of the air/glass/SS410 three phase boundaries was investigated by SEM and is shown in Fig. 8. It shows that after 42 thermal cycles, intensive reaction occurred at the glass/SS410 interface, as shown in Fig. 8(a). Fig. 9 is the EDX line analysis for the glass/SS410 interface in Fig. 8(a). It is noticed from Fig. 9 that the newly formed phase was rich in Ba and Cr. According to Yang et al. [15], $BaCrO_4$ can be formed at/near three phase boundaries (where air, glass and SS410 meet) through the following reaction:

$$Cr_2O_3 + 2BaO + 1.5O_2 = 2BaCrO_4(s) \quad (4)$$

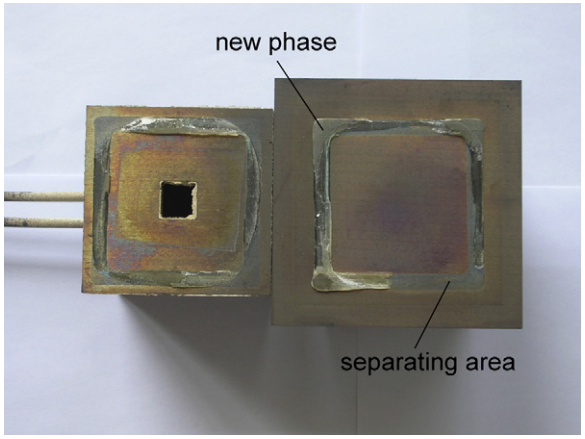

Fig. 6. A photo of the fixture after 42 thermal cycles.

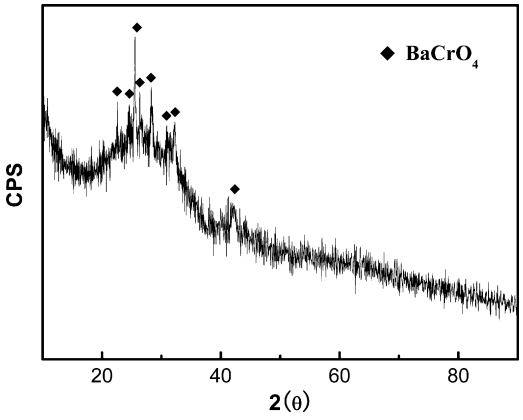

Fig. 7. A XRD pattern of the peeling glass after 42 thermal cycles.

According to the XRD result in Fig. 7 and reaction (4), it can be concluded that the new phase formed at the glass/SS410 interface is $BaCrO_4$. In addition to the $BaCrO_4$ formation reaction at/near the air/glass/SS410 three phase boundaries, the formation of $BaCrO_4$ was also found in the glass surface far from the SS410 as shown in Fig. 8 (a), indicating that Cr species possibly migrated from the SS410 to the glass surface through gas phases. As reported by Hilpert et al. [26], 15 chromium-containing vapor species, i.e. chromium oxide (CrO_i, i = 1–3), hydroxide ($Cr(OH)_j$, j = 1–6) and oxyhydroxide ($CrO(OH)_k$, k = 1–4, $CrO_2(OH)_m$, m = 1–2), can be formed over Cr_2O_3 (s) in humid air. According to the thermodynamic data reported by Ebbinghaus [27] and the method of Gibbs energy minimization, the equilibrium partial pressures over Cr_2O_3 (s) in the humid air (700 °C, $P_{H_2O} = 9.45 \times 10^2$ Pa) was calculated and is shown in Table 1. The equilibrium partial pressures over Cr_2O_3 (s) in another humid air (727 °C, $P_{H_2O} = 2 \times 10^3$ Pa) was also calculated for comparison. It is noticed from Table 1 that the partial pressure of $CrO_2(OH)_2$ is far higher than those of other species. Hilpert et al. [26] also calculated the equilibrium partial pressures over Cr_2O_3 (s). Their results shows that three most abundant vapor species over Cr_2O_3(s) are, respectively, $CrO_2(OH)_2$, CrO_3 and CrO_2OH between 727 °C and 1127 °C in humid air (relative humidity of 60% at 25 °C, corresponding to H_2O partial pressure of 2×10^3 Pa). At 727 °C, the partial pressures of $CrO_2(OH)_2$, CrO_3 and CrO_2OH in the condition ($P_{O_2} = 2.13 \times 10^4$ Pa, $P_{H_2O} = 2 \times 10^3$ Pa) are about 2×10^{-2} Pa, 2×10^{-5} Pa, 4×10^{-6} Pa, respectively. It is noticed that our result is very close to the result reported by Hilpert et al. Therefore, the dominant chromia vapor species over Cr_2O_3 (s) might be $CrO_2(OH)_2$ at 700 °C when moisture is present. According to Yang et al. [15], chromium oxyhydroxide [$CrO_2(OH)_2$] can also react with barium oxide in the sealing glass to form $BaCrO_4$ via the following reaction:

$$CrO_2(OH)_2(g) + BaO(s) = BaCrO_4(s) + H_2O(g) \quad (5)$$

The $BaCrO_4$ in the surface of the glass was possibly formed via reaction (5).

A high magnification SEM image of the glass/SS410 interface in Fig. 8(a) is shown in Fig. 8(b), which shows that the separation occurred from the edge area to the interior area along with the presence of $BaCrO_4$ at the glass side. It is also noticed from Fig. 8(b) that no separation occurred where little $BaCrO_4$ was formed. Therefore, the separation between the glass and SS410 must have a relationship with the formation of $BaCrO_4$ new phase.

Barium chromate possesses a high TEC at $\alpha_a = 16.5 \times 10^{-6}\,K^{-1}$, $\alpha_b = 33.8 \times 10^{-6}\,K^{-1}$, and $\alpha_c = 20.4 \times 10^{-6}\,K^{-1}$ in the temperature range 20–813 °C [15], which is higher than that of the glass and SS410. The large mismatches in TEC among the $BaCrO_4$, glass and SS410 can result in thermal stress in the bulk of the glass, at the glass/$BaCrO_4$ interface and at the $BaCrO_4$/SS410 interface upon heating and cooling. Due to the "self-healing" behavior of the glass, the cracks in the bulk of the glass and at the glass/SS410 interface can heal at operating temperature (700 °C) as long as the annealing time is enough long. However, the cracks at the $BaCrO_4$/SS410 interface can never heal, which resulted in the separation between the glass and SS410, as shown in Fig. 8(b).

The microstructure of the entirely separating glass/SS410 interface was also investigated by SEM and is shown in Fig. 10. Due to the large thermal stress, most of the reaction products had peeled from the glass, which made it difficult to investigate the microstructure changes. However, we still observed the presence of some $BaCrO_4$ new phase in the glass as shown in Figs. 10 and 11.

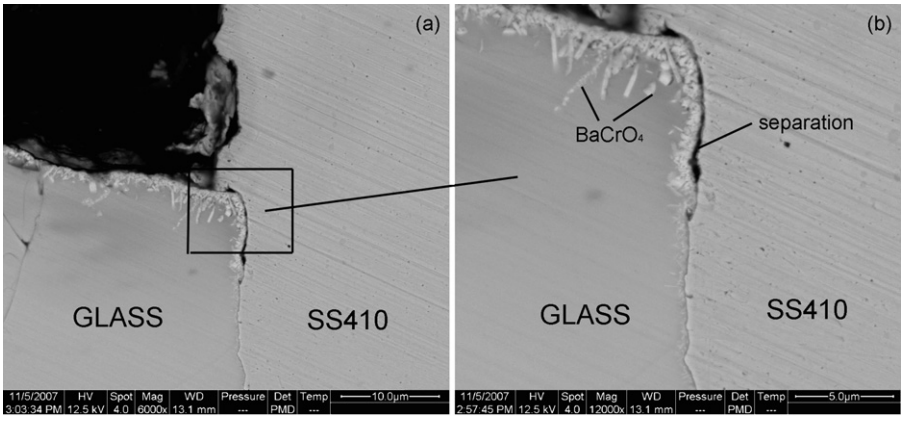

Fig. 8. SEM micrographs of the air/glass/SS410 three phase boundaries after 42 thermal cycles: (a) a low magnification and (b) a high magnification of the marked area in (a).

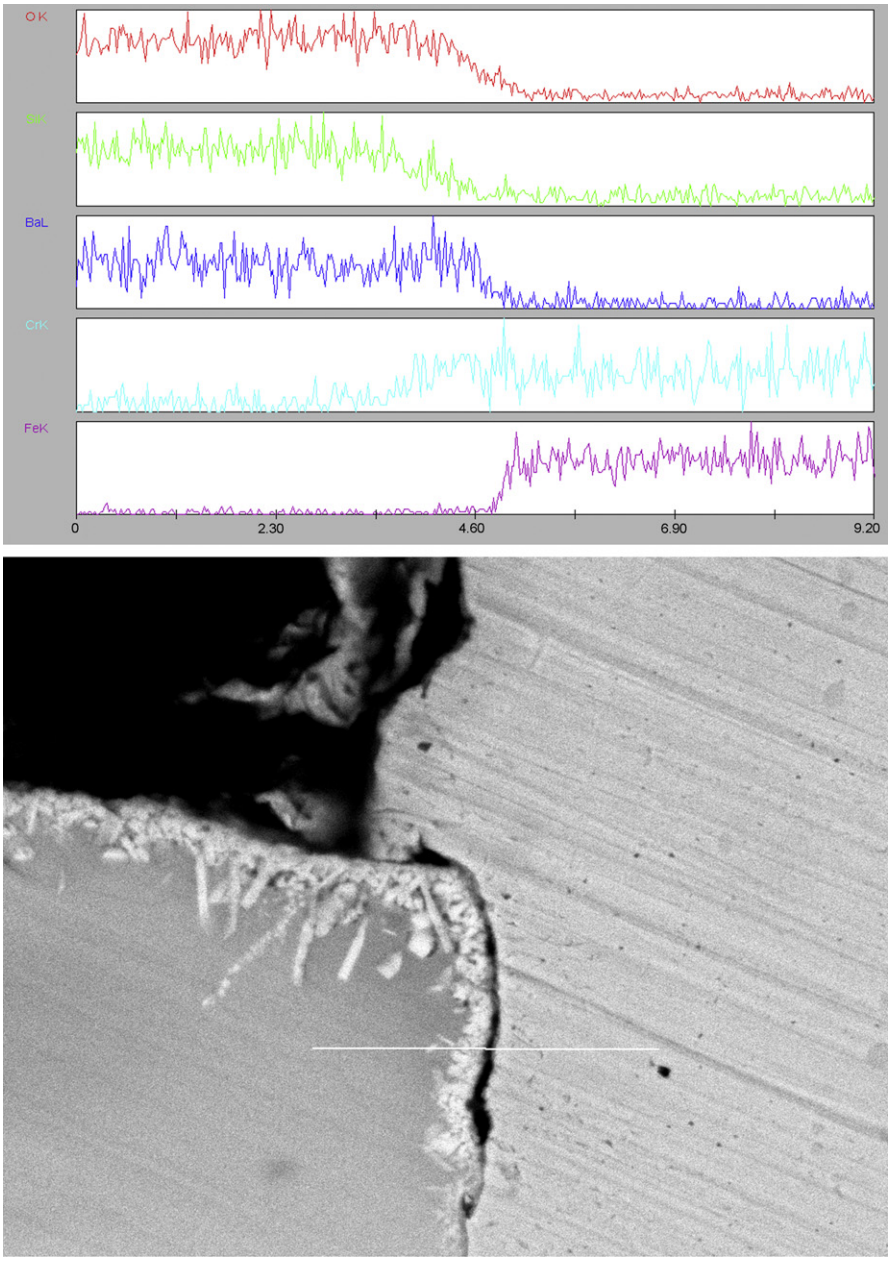

Fig. 9. Linear EDX analysis for the glass/SS410/air three phase boundaries after 42 thermal cycles.

According to the above analyses, the degradation mechanism of the leak rates in Fig. 4 may be deduced as the following:

(1) In the first stage (0th–29th thermal cycle), the leak rates increased slowly from 1.8×10^{-4} sccm cm^{-1} (0th cycle) to 5.8×10^{-3} sccm cm^{-1} (29th cycle), which was caused by the incomplete self-healing behavior of the glass. Crack healing is a dynamic process and the speed of healing would be dependent on the viscosity of glass at a healing temperature. Singh [21] found that the speed of healing was different for various glasses. The glass with lower transition temperature needs shorter time for self-healing at a temperature above T_g. Higher temperature and longer annealing time is helpful to self-healing. The softening temperature of our glass is 662 °C, so the viscosity of our glass is a little high for self-healing at 700 °C. The cracks formed in the bulk of the glass was not completely healed after being annealed at 700 °C only for 1 h, so the leak rates increased with thermal cycles. If the glass was annealed at a higher temperature or for longer time, the leak rates would return to the background leak rate (0th) during initial 29 thermal cycles.

Table 1
Equilibrium partial pressures of most abundant Cr containing species over Cr_2O_3 (s) in humid air ($P_{O_2} = 2.13 \times 10^4$ Pa).

Species (gas)	Equilibrium partial pressures (Pa)	
	700 °C, $P_{H_2O} = 9.45 \times 10^2$ Pa	727 °C, $P_{H_2O} = 2 \times 10^3$ Pa
$CrO_2(OH)_2$	1.03×10^{-2}	2.59×10^{-2}
CrO_3	1.30×10^{-5}	2.77×10^{-5}
$CrO_2(OH)$	1.89×10^{-6}	6.10×10^{-6}
$CrO(OH)_3$	1.44×10^{-7}	6.92×10^{-7}
$CrO(OH)_2$	7.25×10^{-8}	3.51×10^{-7}

(2) The second stage is the 29th–42nd thermal cycle, where the leak rates increased rapidly from 5.8×10^{-3} sccm cm^{-1} (29th cycle) to 5.5×10^{-2} sccm cm^{-1} (42nd cycle). In this stage, due to the occurrence of reaction (4), the accumulation of barium chromate in the interfacial zone likely resulted in the

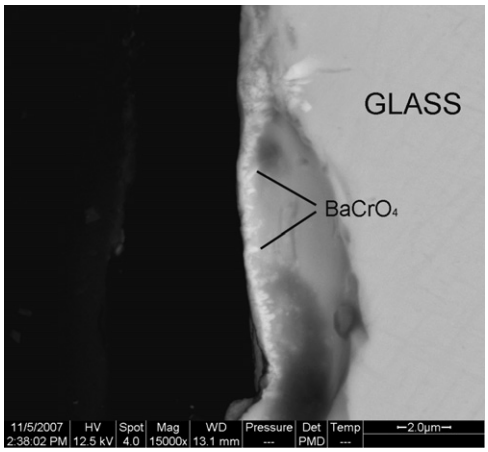

Fig. 10. A SEM micrograph of the entirely separating glass/SS410 interface after 42 thermal cycles.

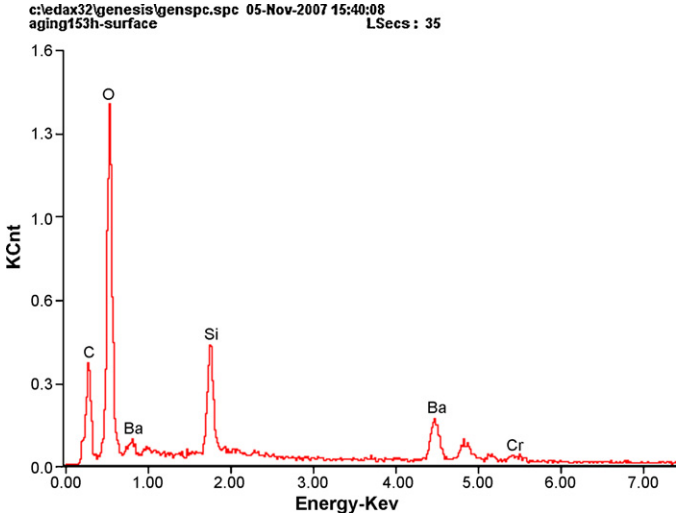

Fig. 11. A result of EDX analysis at the new phase in Fig. 10.

cracks between the $BaCrO_4$ and SS410 during heating and cooling due to the large thermal expansion mismatch. The cracks between the $BaCrO_4$ and SS410 can never heal at operation temperature. Therefore, air could diffuse into the internal area along the cracks, which accelerated the growth of the internal barium chromate. When the growth of the internal barium chromate reached a critical scale, new cracks occurred between the $BaCrO_4$ and SS410 during heating and cooling. As a result, the crack tips propagated with thermal cycles until the continuous cracks were formed, which resulted in the rapid increase of the leak rates.

In conclusion, the initially slow increase of the leak rates was caused by the incomplete self-healing behavior of the glass, however, the subsequently rapid increase of the leak rates was caused by the formation of more and more leak paths. According to the above analyses, the leak paths must be formed as follows: $BaCrO_4$ was formed at the air/glass/SS410 three phase boundaries → cracks occurred at the three phase boundaries during thermal cycling due to the large TEC mismatch → air diffused into the internal area along the cracks → $BaCrO_4$ was formed at the internal area → cracks occurred at the internal area during thermal cycling due to the large TEC mismatch → $BaCrO_4$ was formed at the entire glass/SS410 interface → cracks were formed at the entire glass/SS410 interface during thermal cycling due to the large TEC mismatch → leak paths were formed. Therefore, it is thought to be the degradation mechanism of the thermal cycle stability that the formation of more and more $BaCrO_4$ at the glass/SS410 interface resulted in the larger and larger leak paths with thermal cycles.

4. Conclusions

In this paper, the thermal cycle stability of a thermally stable sealing glass was investigated with a SS410 fixture from 150 °C to 700 °C. The leak rates of the glass at 700 °C increased with thermal cycles and appeared to be two different stages. In the first stage, the leak rates increased slowly with thermal cycles, which was caused by the incomplete self-healing behavior of the glass. In the second stage, the leak rates increased rapidly with thermal cycles, which was caused by the formation of the $BaCrO_4$ new phase. Because of the large TEC mismatch among the $BaCrO_4$, SS410 and glass, cracks occurred during thermal cycling. With the formation of more and more $BaCrO_4$ at the glass/SS410 interface, the crack tips continually propagated into the internal area. As a result, more and more continuous leak paths were formed with thermal cycles, which resulted in the rapid increase of the leak rates in the second stage. As reported in an earlier paper [22], the glass has good chemical compatibility with 8YSZ, so 8YSZ coating can be sprayed on the surface of the SS410 to inhibit the formation of the $BaCrO_4$ new phase, which can improve the long-term thermal cycle stability of the glass.

Acknowledgements

The financial support from National Natural Science Foundation of China under the Contract Nos. 50730002 and 20876159 is highly appreciated.

References

[1] Y.S. Chou, J.W. Stevenson, J. Hardy, P. Singh, J. Power Sources 157 (2006) 260–270.
[2] Y.S. Chou, J.W. Stevenson, J. Power Sources 140 (2005) 340–345.
[3] K.L. Ley, M. Krumpelt, R. Kumar, J.H. Meiser, I. Bloom, J. Mater. Res. 11 (6) (1996) 1489–1493.
[4] C. Lara, M.J. Pascual, M.O. Prado, A. Durán, Solid State Ionics 170 (2004) 201–208.
[5] P.A. Lessing, J. Mater. Sci. 42 (2007) 3465–3476.
[6] C. Lara, M.J. Pascual, A. Durán, J. Non-Cryst. Solids 348 (2004) 149–155.
[7] Y.S. Chou, J.W. Stevenson, J. Power Sources 112 (2002) 376–383.
[8] S.P. Simner, J.W. Stevenson, J. Power Sources 102 (2001) 310–316.
[9] K.S. Weil, JOM 58 (8) (2006) 37–44.
[10] K.S. Weil, C.A. Coyle, J.T. Darsell, G.G. Xia, J.S. Hardy, J. Power Sources 152 (2005) 97–104.
[11] M. Brochu, B.D. Gauntt, R. Shah, G. Miyake, R.E. Loehman, J. Eur. Ceram. Soc. 26 (5) (2006) 3307–3313.
[12] Y.S. Chou, J.W. Stevenson, P. Singh, J. Electrochem. Soc. 154 (7) (2007) B644–B651.
[13] S.B. Sohn, S.Y. Choi, G.H. Kim, H.S. Song, G.D. Kim, J. Am. Ceram. Soc. 87 (2) (2004) 254–260.
[14] K.S. Weil, J.E. Deibler, J.S. Hardy, D.S. Kim, G.G. Xia, L.A. Chick, C.A. Coyle, J. Mater. Eng. Perform 13 (3) (2004) 316–326.
[15] Z.G. Yang, J.W. Stevenson, K.D. Meinhardt, Solid State Ionics 160 (2003) 213–225.
[16] N. Lahl, D. Bahadur, K. Singh, L. Singheiser, K. Hilpert, J. Electrochem. Soc. 149 (5) (2002) A607–A614.
[17] Z.G. Yang, K.D. Meinhardt, J.W. Stevenson, J. Electrochem. Soc. 150 (8) (2003) A1095–A1101.
[18] P.H. Larsen, F.W. Poulsen, R.W. Berg, J. Non-Cryst. Solids 244 (1999) 16–24.
[19] P.H. Larsen, P.F. James, J. Mater. Sci. 33 (1998) 2499–2507.
[20] S.T. Reis, R.K. Brow, J. Mater. Eng. Perform 15 (2006) 410–413.
[21] R.N. Singh, Int. J. Appl. Ceram. Technol. 4 (2) (2007) 134–144.
[22] Q.S. Zhu, L. Peng, T. Zhang, Stable glass seals for intermediate temperature (IT) SOFC applications, in: K. Kuang, K. Easler (Eds.), Fuel Cell Electronics Packaging, Springer Science+Business Media, LLC, New York, 2007, pp. 33–60.
[23] L. Peng, Q.S. Zhu, J. Fuel Cell Sci. Technol. 5 (3) (2008) 031210.
[24] S.P. Jiang, L. Christiansen, B. Hughan, K. Fogen, J. Mater. Sci. Lett. 20 (2001) 695–697.
[25] Y.S. Chou, J.W. Stevenson, P. Singh, J. Power Sources 152 (2005) 168–174.
[26] K. Hilpert, D. Das, M. Miller, D.H. Peck, R. Weiβ, J. Electrochem. Soc. 143 (11) (1996) 3642–3647.
[27] B.B. Ebbinghaus, Combust. Flame 93 (1993) 119–137.